Available online at www.sciencedirect.com

ScienceDirect

Journal of Magnesium and Alloys 11 (2023) 2205–2215

www.elsevier.com/locate/jma

Full Length Article

Ameliorating the re/dehydrogenation behaviour of MgH_2 by zinc titanate addition

N.A. Ali[a], N.A. Sazelee[a], M.F. Md Din[b], M.M. Nasef[c,d], A.A. Jalil[c,e], Haizen Liu[f,g], M. Ismail[a,c,*]

[a] *Energy Storage Research Group, Faculty of Ocean Engineering Technology and Informatics, Universiti Malaysia Terengganu, 21030 Kuala Nerus, Terengganu, Malaysia*

[b] *Department of Electrical and Electronic Engineering, Faculty of Engineering, National Defence University of Malaysia, Kem Sungai Besi, Kuala Lumpur, Malaysia*

[c] *Center of Hydrogen Energy, Institute of Future Energy, Universiti Teknologi Malaysia, 81310 UTM Johor Bahru, Johor, Malaysia*

[d] *Department of Chemical and Environmental Engineering, Malaysia Japan International Institute of Technology, Universiti Teknologi Malaysia, Jalan Sultan Yahya Petra, Kuala Lumpur 54100, Malaysia*

[e] *Faculty of Chemical and Energy Engineering, Universiti Teknologi Malaysia, 81310 UTM Johor Bahru, Johor, Malaysia*

[f] *Guangxi Novel Battery Materials Research Center of Engineering Technology, State Key Laboratory of Featured Metal Materials and Life-cycle Safety for Composite Structures, School of Physical Science and Technology, Guangxi University, Nanning 530004, China*

[g] *State Key Laboratory of Featured Metal Materials and Life-cycle Safety for Composite Structures, Nanning 530004, China*

Received 16 January 2023; received in revised form 10 May 2023; accepted 24 May 2023
Available online 7 June 2023

Abstract

Magnesium hydride (MgH_2) is the most feasible and effective solid-state hydrogen storage material, which has excellent reversibility but initiates decomposing at high temperatures and has slow kinetics performance. Here, zinc titanate (Zn_2TiO_4) synthesised by the solid-state method was used as an additive to lower the initial temperature for dehydrogenation and enhance the re/dehydrogenation behaviour of MgH_2. With the presence of Zn_2TiO_4, the starting temperature for the dehydrogenation of MgH_2 was remarkably lowered to around 290 °C–305 °C. In addition, within 300 s, the MgH_2–Zn_2TiO_4 sample absorbed 5.0 wt.% of H_2 and 2.2–3.6 wt.% H_2 was liberated from the composite sample in 30 min, which is faster by 22–36 times than as-milled MgH_2. The activation energy of the MgH_2 for the dehydrogenation process was also downshifted to 105.5 kJ/mol with the addition of Zn_2TiO_4 indicating a decrease of 22% than as-milled MgH_2. The superior behaviour of MgH_2 was due to the formation of $MgZn_2$, MgO and $MgTiO_3$, which are responsible for ameliorating the re/dehydrogenation behaviour of MgH_2. These findings provide a new understanding of the hydrogen storage behaviour of the catalysed-MgH_2 system.

Keywords: Hydrogen storage; Solid-state storage; MgH_2; Additive; Zn_2TiO_4.

1. Introduction

Hydrogen has recently drawn global interest as an energy carrier for the future because of its abundant resources and environmentally friendly. The need for safe and effective hydrogen storage is essential for the use of onboard hydrogen applications. Among the several methods of storing hydrogen available (e.g. solid-state, liquid and gaseous), storing hydrogen via solid-state approaches is one of the most superior, efficient and safe. Magnesium hydride (MgH_2) is one of the most effective solid-state materials owing to its abundance as well as its light weight, low cost and high hydrogen concentration (7.6 wt.% gravimetric and 110-g/L volumetric) [1–4]. Unfortunately, the temperature for the release of hydrogen is high (>400 °C), and the desorption kinetics are slowly caused by the high desorption enthalpy ($\Delta H = 76$ kJ/mol H_2) [5,6].

* Corresponding author.
E-mail address: mohammadismail@umt.edu.my (M. Ismail).

https://doi.org/10.1016/j.jma.2023.05.005

Multifarious methods have been applied (e.g. alloying, nanosizing, doping with additives and destabilising with other hydrides) to accelerate the re/dehydrogenation kinetics and reduce the operating temperature of MgH_2 [7–15]. Particularly, additive doping has been regarded as the most efficient strategy to tackle the drawbacks of MgH_2. The introduction of an additive, such as carbon material, rare metal-based material and transition metal-based material into MgH_2, results in the superior performance of MgH_2 [16–19]. Among them, transition metal and their compounds have received special attention because of the distinctive electronic structure that might debilitate the Mg–H bond which then accelerates the dehydrogenation process of MgH_2 [20]. It has been observed that 3d transition metals (e.g. Ni, Cu, Co, Ti and Fe) have the effect of weakening the Mg–H bond because of their distinct electron configurations with the d-band, hence promoting H_2 molecule dissociation and recombination on the Mg/MgH_2 surface [21]. Moreover, according to first-principle calculations, transition metal additives (Ti, Ni, Fe and Co) can create a change in the Fermi level, which improves MgH_2 desorption rates [22]. Further, Rahwanto et. al [23] showed that the addition of Ni resulted in a high surface area composite with finely dispersed Ni particles on the surface of Mg that led to a significant improvement in the kinetic performance of the MgH_2–Ni. The addition of Ti was also found to accelerate the kinetics of MgH_2 with the ability to absorb 2.7 wt.% H_2 in less than 7 min [24].

The hydrogen storage properties of MgH_2 can be also synergized by adding a double catalyst consisting of SiC and Ni. The former improves the kinetics of H_2 absorption/desorption in MgH_2, while the latter acts as a hydrogenation catalyst. The decomposition temperature of the MgH_2–SiC–Ni was downshifted to 250 °C and the composite sample was able not only to absorb 5.7 wt.% H_2 but also to release the same amount of $\%H_2$ in 8.3 min [25]. The improved absorption kinetics of the MgH_2–SiC–Ni sample was attributed to the smaller particle size that led to a large contact area between the sample and remarkably increase the absorption rate [25,26]. In another study, Chen et al. [27] demonstrated that the addition of transition metal oxide (ZrO_2) with carbon significantly improve the hydrogen storage performance of MgH_2. One of the key improvements observed in MgH_2–ZrO_2/C was the downshift of the onset decomposition temperature to 208 °C. The density functional theory (DFT) calculations that was conducted to support the experimental results proved that the addition of ZrO_2/C weakened the Mg–H bonding strength and lowered the desorption energy leading to excellent hydrogen storage properties of MgH_2 at moderate temperature. Moreover, other studies demonstrated that the composite of Mg–Nb_2O_5–C are beneficial in lowering the desorption temperature of MgH_2 and also reduced the activation energy [28]. In addition, Milanese et al. [29] showed that adding TiO_2 to the Mg–Ni–C composite resulted in a decrease of the dehydrogenation temperature. They indicated that the addition of TiO_2 increase the sorption efficiency of the active phases and is responsible for the improved sorption rates.

Ti-based additives, among the transition metal, are significant in accelerating the performance of MgH_2 [30–32]. In particular, Hu et al. [33] found that the Ti compound ($K_2Ti_8O_{17}$) could decrease the operating temperature of MgH_2 to 189 °C and maintain excellent capacity retention (88%) after completing the eight cycles. Another study also indicated that adding $K_2Ti_6O_{13}$ resulted in the tremendous performance of MgH_2 because of the positive synergetic function of TiO_2, Ti and $KMgH_3$ during the heating process [34]. At 280 °C, the $K_2Ti_6O_{13}$-doped MgH_2 sample rapidly desorbs 6.7 wt.% H_2 in 3 min and lower the dehydrogenation activation energy to 105.67 kJ/mol. Thereafter, Shao et al. [35] introduced TiO_2 into MgH_2 and resulting in superior performance. At 100 °C, the TiO_2-doped MgH_2 sample rapidly absorbs 4.17 wt.% H_2 in 30 min and liberates 5.75 wt.% H_2 in 16.7 min at 300 °C. The significant improvement of the TiO_2-doped MgH_2 sample was ascribed to the ultrafine and uniformly scattered TiO_2 particle that offers a high number of reactive sites for ab/desorption of MgH_2.

Another study has shown that the addition of TiO_2 nanosheets (NS) can improve the kinetics performance of MgH_2 [36]. The MgH_2–TiO_2 (NS) sample was able to release 1.2 wt.% H_2 within 300 min at low temperature of 180 °C. This was accompanied by a significant improvement in the absorption kinetics of MgH_2–TiO_2 (NS) that allowed the sample to absorb 6.1 wt.% H_2 within 10 s at 150 °C. Furthermore, a study conducted by Zhang et al. [37] demonstrated enhanced hydrogen storage performance of MgH_2 with monodispersed single-crystal-like TiO_2 wrapped with amorphous carbon (MgH_2–TiO_2 SCNPs/AC). The MgH_2–TiO_2 SCNPs/AC sample attained lower operating temperature and activation energy and exhibited faster kinetics with the ability to be fully rehydrogenated with a reversible capacity of 6.5 wt.% H_2 within 5 min at 200 °C. A recent work has reported that adding graphene-like TiO_2 (B) imparted an excellent catalytic effect to the performance of MgH_2 [38]. The MgH_2–TiO_2 (B) sample started to release hydrogen at 200 °C and desorbed 6.88 wt.% H_2 below 288 °C. The enhanced performance of the MgH_2–TiO_2 (B) sample was ascribed to the reduction of TiO_2 (B) nanosheets to the metallic Ti nanoparticles and wrinkled Ti_2O_3 during the ball milling and dehydriding processes, resulting in many boundary contacts between MgH_2 and Ti-based catalysts, which collectively promoted hydrogen diffusion.

Inspired by the above kinds of literature, it is interesting to explore another Ti-based additive, which is Zn_2TiO_4. Recently, Zn_2TiO_4 has demonstrated promising performance as an lithium-ion battery anode material [39]. Apart from that, Zn_2TiO_4 also showed an excellent catalytic effect as an electrode sensor for UV photocatalysts [40]. Therefore, it is believed that Zn_2TiO_4 will result in superior performance for the hydrogen storage application. Herein, Zn_2TiO_4 was utilised as an additive to boost the re/dehydrogenation behaviour of MgH_2. To date, no study has been conducted on the impact of Zn_2TiO_4 on the re/dehydrogenation behaviour of MgH_2. In this study, the Zn_2TiO_4 was synthesised by using solid-state method, and various weight percentages (wt.%) of Zn_2TiO_4

were introduced to MgH_2. The specific mechanism of the MgH_2–Zn_2TiO_4 system was discussed in depth in this study.

2. Experimental details

Pure MgH_2 (95%), ZnO (99.9%, <100 nm), anatase TiO_2 (99.95%, 21 nm) and ammonia solution were commercially purchased from Sigma Aldrich. The Zn_2TiO_4 was synthesized by using solid-state method. The ZnO and TiO_2 were ground together in stochiometric amounts using agate mortar for 15 min. Thereafter, a few drops of ammonia solution were added drop by drop to increase the reaction rate during the synthesis process as reported elsewhere [41,42]. The mixture was ground again for another 15 min and then the mixture was subsequently dried for 5 h at 60 °C and annealed at 1000 °C for 3 h. In order to examine the hydrogen storage behaviour of MgH_2, various amount of the as-synthesised Zn_2TiO_4 (5, 10, 15 and 20 wt.%) was then mixed with MgH_2 via planetary ball mill (NQM-0.4) for 1 h. To minimise oxidation, the sample was prepared in a Mbraun glovebox with Argon gas flowing through it.

The composition of the samples was identified using Rigaku MiniFlex X-ray diffractometer (XRD) with Cu Kα radiation. For each measurement, the samples were scanned over diffraction angles of $20° < 2\theta < 80°$ with a speed of 2°/min. The Shimadzu IR Tracer-100 was used to perform the Fourier-transform infrared (FT-IR) measurement between 400 and 2000 cm^{-1} at a resolution of 4 cm^{-1} with a scanning capable of 20 spectra/second, equipped with Attenuated total reflectance (ATR) mode and scanning electron microscopy (SEM; JEOL JSM-6360LA) was employed to investigate the microstructures and morphologies of the samples. Renishaw Raman spectrometer was used to conduct Raman spectra at ambient temperature with a 0.1% power laser (532 nm radiation). The measurement was conducted between 100 to 1000 cm^{-1} with a spectral resolution of <2.5 cm^{-1} in an air atmosphere. For FT-IR and Raman, to minimise the exposure to air and moisture, the sample was placed in microcentrifuge tubes (1.5 mL) during transportation from the glove box.

The hydrogen storage behaviour of MgH_2–Zn_2TiO_4 was evaluated using a Sievert-type apparatus from Advanced Materials (pressure–composition–temperature (PCT)). The sample was heated from room temperature to 450 °C to determine the starting dehydrogenation temperature. The dehydrogenation and rehydrogenation kinetics experiments were performed at 300 and 320 °C (1 atm H_2 pressure) and 250 and 320 °C (33 atm H_2 pressure), respectively. The differential scanning calorimetry (DSC) was tested using TGA/DSC 1, Mettler Toledo in the temperature range from room temperature to 550 °C at varied rates (15 to 30 °C/min). For comparison, all of the characterizations were also performed on as-milled MgH_2.

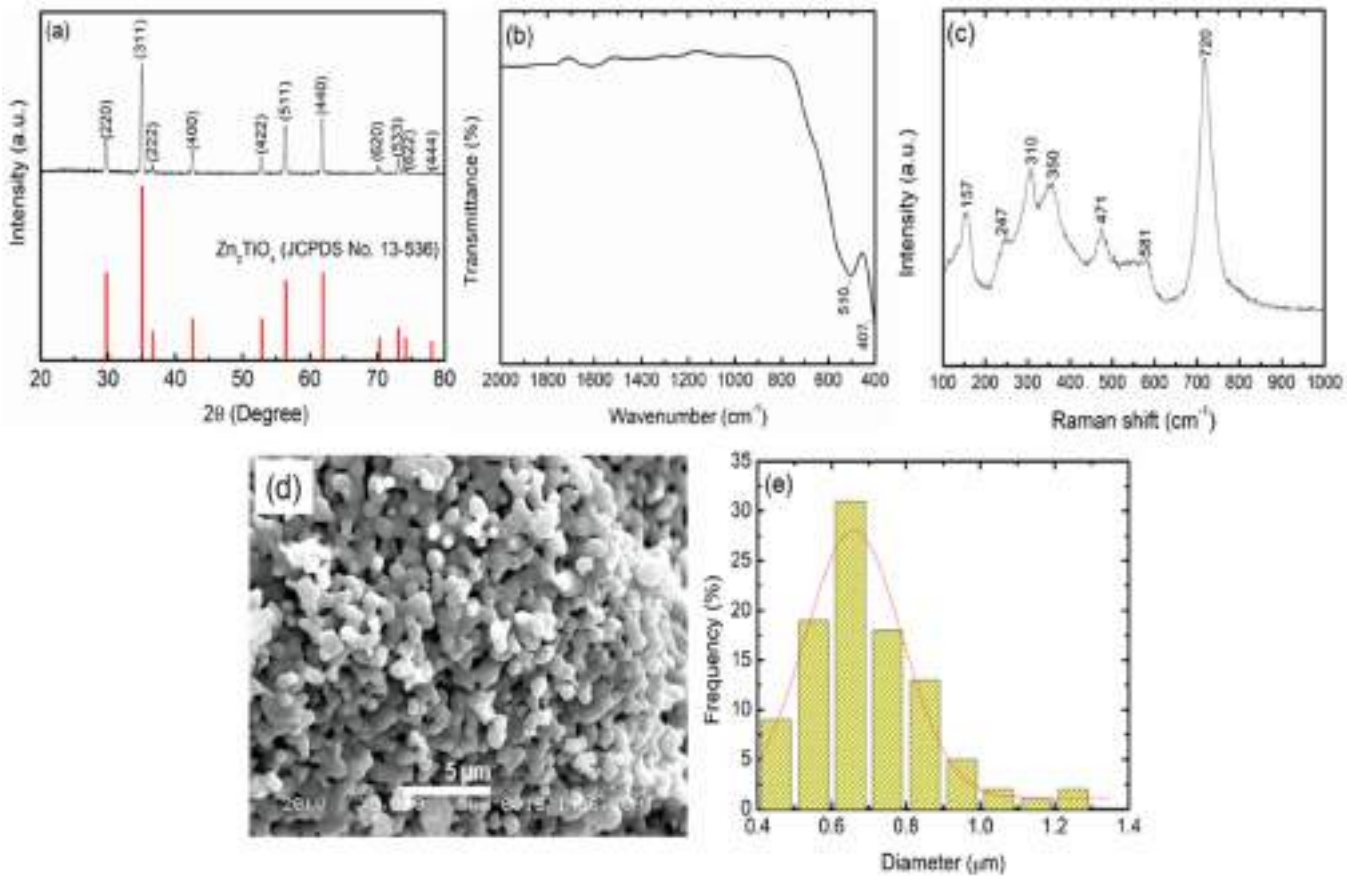

Fig. 1. The (a) XRD pattern, (b) FT-IR profile, (c) Raman profile, (d) micrograph and (e) particle size distributions of the Zn_2TiO_4.

3. Results and discussions

3.1. Synthesis of Zn_2TiO_4

The crystallographic structure of the Zn_2TiO_4 was examined by using XRD as demonstrated in Fig. 1(a). The XRD spectra of the as-synthesised Zn_2TiO_4 were perfectly indexed with the Zn_2TiO_4 phase (JCPDS 13-536), confirming the high purity of Zn_2TiO_4. The diffraction peaks of 2θ at 29.7°, 35.0°, 36.6°, 42.6°, 52.9°, 56.4°, 61.9°, 70.3°, 73.1°, 74.2° and 78.0° are ascribed to the (220), (311), (222), (400), (422), (511), (440), (620), (533), (622) and (444) planes of Zn_2TiO_4. The mean crystallite size of the Zn_2TiO_4 was determined to be 26.7 nm using the Scherrer equation as in Eq. 1 [43]:

$$L = K\lambda/\beta\cos\theta \quad (1)$$

whereas

L = mean size of the crystallite
K = Scherer constant
λ = X-ray wavelength
β = full width at half maximum (FWHM)
θ = diffraction angle

Fig. 1(b) shows the FT-IR spectra of Zn_2TiO_4 which present the standard bands of Zn_2TiO_4, that occur at 407 and 510 cm^{-1} and correlate to the Ti–O and Zn–O bond, respectively [44]. Additional characterisation performed by Raman spectroscopy as in Fig. 1(c) showed the typical peaks of Zn_2TiO_4. The peaks at 247, 310, 350, 471 and 720 cm^{-1} are assigned to the spinel structure of Zn_2TiO_4 [45]. The Raman mode at 581 cm^{-1} was attributed to the order–disorder effect of Zn and Ti ions while the peaks at 157 cm^{-1} were due to the laser-induced plasma effect [46,47]. The morphology of the as-synthesised Zn_2TiO_4, which consists of spherical particle that seems to be generally uniform, is shown in Fig. 1(d). The mean particle size of the Zn_2TiO_4 evaluated by the Image J software as represented in the histogram (Fig. 1(e)) was 0.65 μm.

3.2. Hydrogen storage behaviour of MgH_2–Zn_2TiO_4 system

As depicted in Fig. 2(a), the influence of Zn_2TiO_4 on the hydrogen storage behaviour of MgH_2 was scrutinised by the TPD (temperature–programmed–desorption). The initial dehydrogenation temperature for the commercial MgH_2 happened at around 405 °C and released 7.2 wt.% H_2. Subsequently, the

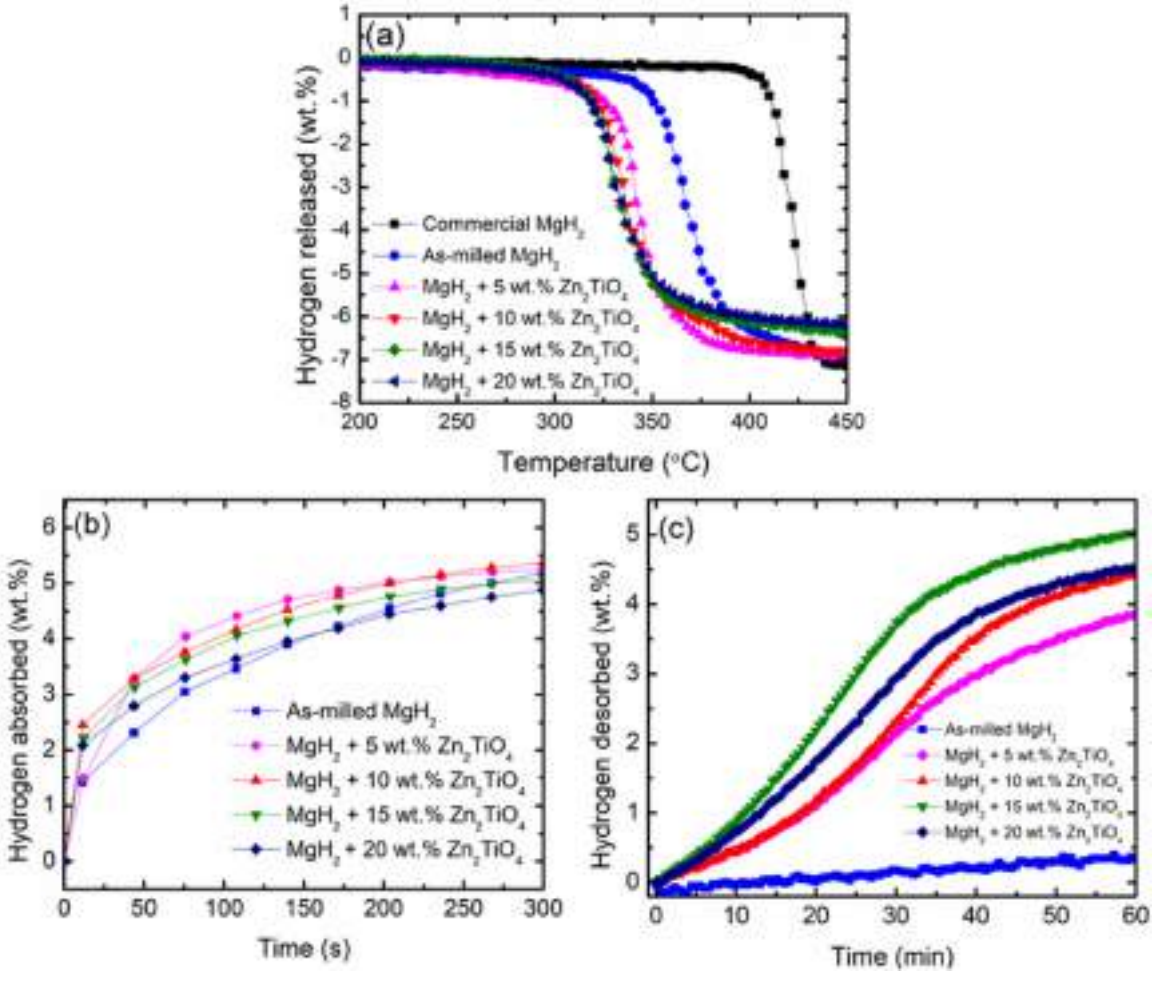

Fig. 2. (a) TPD curves, (b) rehydrogenation curve at 250 °C and (c) dehydrogenation curve at 300 °C of MgH_2 + Xwt.% Zn_2TiO_4 (X = 5, 10, 15 and 20).

Table 1
Comparison of the hydrogen storage performance of $MgH_2 + Zn_2TiO_4$ sample with other additives synthesized via the solid-state method.

System	Decomposition temperature (°C)	Absorption capacity (wt.%)	Desorption capacity (wt.%)	Reference
MgH_2– $BaFe_{12}O_{19}$	270	4.3 wt.% in 10 min at 150 °C	3.4 wt.% in 15 min at 320 °C	[48]
MgH_2–$CoTiO_3$	275	6.4 wt.% in 10 min at 200 °C	5.5 wt.% in 30 min at 300 °C	[49]
MgH_2–$LaFeO_3$	300	6.1 wt.% in 60 min at 150 °C	3.7 wt.% in 30 min at 320 °C	[17]
MgH_2–Zn_2TiO_4 (this system)	290	4.1 wt.% in 1.7 min at 250 °C	4.8 wt.% in 60 min at 300 °C	Current study

initial dehydrogenation temperature of MgH_2 was decreased to 340 °C after 1 h of milling suggesting that the milling procedure contributed to the reduction of the dehydrogenation temperature of MgH_2. The amount of hydrogen released from the as-milled MgH_2 was 7.0 wt.%. Furthermore, the initial temperature for the dehydrogenation of MgH_2 was lowered significantly by adding different weight percentages of Zn_2TiO_4. The MgH_2 + 5 wt.% Zn_2TiO_4 sample commenced desorbing hydrogen at 305 °C, releasing a 6.9 wt.% of H_2. Then, by varying the amount of Zn_2TiO_4 to 10, 15, and 20 wt.%, the initial dehydrogenation temperature was reduced to roughly 290 °C. The amounts of hydrogen released for the 10, 15, and 20 wt.%-doped MgH_2 samples was 6.8, 6.4 and 6.1 wt.%, respectively. This finding suggests that an increased amount of additive lowers the initial dehydrogenation temperature even further. Moreover, the results demonstrated that the addition of Zn_2TiO_4 is promising for the downshift of the initial dehydrogenation temperature of MgH_2. Table 1 shows a comparison between the hydrogen storage performance of the MgH_2 + Zn_2TiO_4 system in the present study and composites obtained by the same method with other additives and reported in literature.

Then, the different weight percentage of Zn_2TiO_4 was milled together with MgH_2 and their corresponding absorption kinetics curve is displayed in Fig. 2(b) to assess the catalytic performance of the Zn_2TiO_4 on the absorption performance of MgH_2. Based on the figure, in 100 s, the as-milled MgH_2 absorbed 3.3 wt.% H_2 while in the same time duration, the MgH_2 + 5 wt.% Zn_2TiO_4 composite rapidly absorbed 4.4 wt.% H_2 and the 10, 15 and 20 wt.%-doped MgH_2 sample absorbed 4.1 wt.%, 4.0 wt.% and 3.6 wt.% H_2, respectively. All the doped samples present better absorption performance than as-milled MgH_2. Considering the previous study of the MgH_2 with the addition of a TiO_2 sample [35], one can observe that MgH_2–TiO_2 sample absorbed 4.17 wt.% H_2 in 30 min compared to the same amount in 1.7 min for MgH_2–Zn_2TiO_4 sample in the present study. This confirms the presence of acceleration absorption kinetics in the MgH_2–Zn_2TiO_4 sample because of the addition of Zn_2TiO_4. As depicted in Fig. 2(c), further study was done on hydrogen desorption at 300 °C which was recorded for 60 min. From the figure, MgH_2 doping with Zn_2TiO_4 presents the highest amount of hydrogen desorbed. The amount of hydrogen desorbed within the first 30 min for the as-milled MgH_2 sample was 0.1 wt.%. The amount of hydrogen desorbed was significantly high by doping with a various amount of Zn_2TiO_4. The amount of hydrogen desorbed for the 5, 10, 15 and 20 wt.% Zn_2TiO_4-doped MgH_2 in 30 min was 2.2, 2.5, 3.6 and 3.0 wt.% H_2, respectively, which is 22–36 times more rapidly than as-milled MgH_2. Even after 1 h, the as-milled MgH_2 was unable to reach the same high capacity as the MgH_2–Zn_2TiO_4 sample. The MgH_2–Zn_2TiO_4 sample desorbed 3.8, 4.4, 4.8 and 4.5 wt.% H_2 in 60 min for the 5, 10, 15 and 20 wt.% Zn_2TiO_4, respectively, but the as-milled MgH_2 desorbed only 0.3 wt.% H_2. Consequently, the addition of the Zn_2TiO_4 additive (even in a low amount) results in a large improvement in the desorption kinetics of MgH_2. For further analysis, the MgH_2 + 10 wt.% Zn_2TiO_4 sample was selected due to the low dehydrogenation temperature with high hydrogen content and faster absorption/desorption kinetics.

A long-life cycle is a great challenge for hydrogen storage applications. Hence, the cycling performance of the MgH_2 + 10 wt.% Zn_2TiO_4 sample was studied. Temperature of 320 °C were applied in the cycling study of the MgH_2 + 10 wt.% Zn_2TiO_4 sample. Fig. 3(a) and 3(b) presents the cycling performance of the MgH_2 + 10 wt.% Zn_2TiO_4 sample over 10 cycles. For the absorption kinetics, in the 10^{th} cycle, 6.6 wt.% H_2 capacity was maintained which showed a small degradation compared to the 1^{st} cycle (7.0 wt.%). For the desorption kinetics, the capacity for the 1^{st} cycle was 4.6 wt.% H_2. Surprisingly, after the 10 cycles, 4.5 wt.% H_2 was maintained indicating a remarkable stability where the MgH_2 + 10 wt.% Zn_2TiO_4 sample retained 97.8% of the original capacity. The cycling performance indicates that the addition of Zn_2TiO_4 is highly beneficial for maintaining the superior cyclability behaviour of MgH_2. Further, the XRD analysis that was carried out on the MgH_2 + 10 wt.% Zn_2TiO_4 samples after completing the 10^{th} cycle depicted in Fig. 3(c) to ascertain the reason for the decreased hydrogen storage capacity. For the dehydrogenated state (Fig. 3(c)(i)), the peaks that were detected were that of Mg coupled with the additional peaks of MgO, $MgTiO_3$ and $MgZn_2$. The peaks of MgO, $MgTiO_3$ and $MgZn_2$ remain unchanged for the rehydrogenated state (Fig. 3(c)(ii)). The presence of Mg suggests a complete dehydrogenation of MgH_2. The formation of MgO, $MgTiO_3$ and $MgZn_2$ is believed to reduce the capacity of the MgH_2 + 10 wt.% Zn_2TiO_4 samples. These findings are in line with the previous study that reported reduced hydrogen capacity due to the formation of active species during cycles [50].

Then, the DSC experiment was used to comprehensively evaluate the dehydrogenation behaviour of the $MgH_2 + Zn_2TiO_4$ sample. Fig. 4 shows the DSC profile of as-milled MgH_2 and MgH_2 + 10 wt.% Zn_2TiO_4 sample (heating rate: 25 °C/min). As indicated in the figure, the endothermic peak of as-milled MgH_2 appeared at 430 °C, while the endothermic peaks of MgH_2 + 10 wt.% Zn_2TiO_4 appeared at 390 °C. The endothermic peaks of the MgH_2 + 10 wt.% Zn_2TiO_4 sample was lower by 40 °C than undoped MgH_2

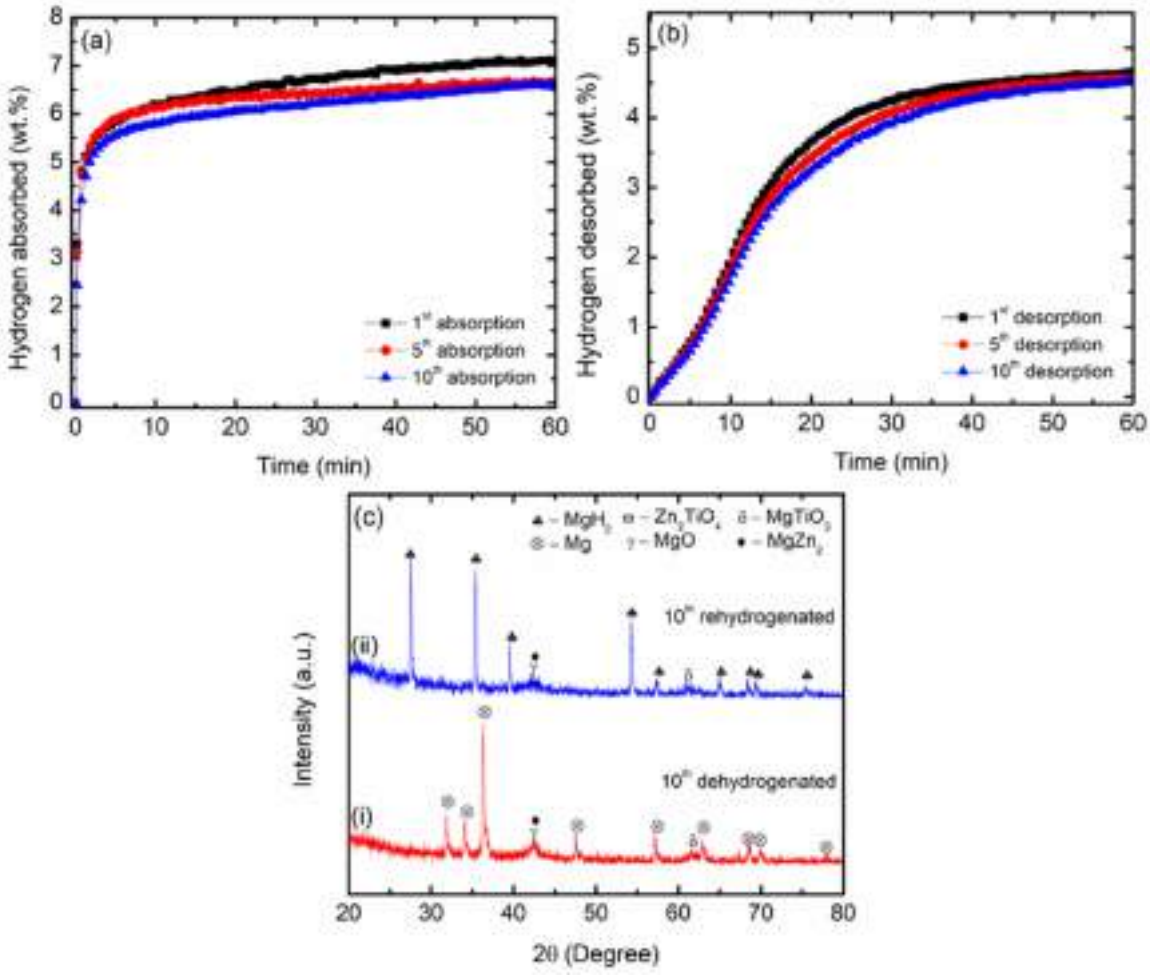

Fig. 3. The (a) rehydrogenation cycling at 320 °C under 33 atm H_2 pressure, (b) dehydrogenation cycling at 320 °C under 1 atm H_2 pressure and (c) XRD patterns of the (i) dehydrogenated and (ii) rehydrogenated sample of MgH_2 + 10 wt.% Zn_2TiO_4 samples after completing the 10^{th} cycle.

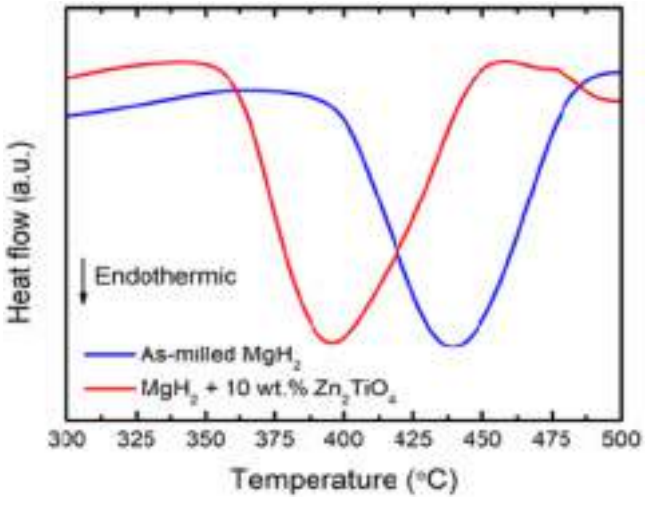

Fig. 4. DSC trace of as-milled MgH_2 and MgH_2 + 10 wt.% Zn_2TiO_4 at 25 °C/min.

indicating an enhancement of the dehydrogenation behaviour of MgH_2 with the inclusion of Zn_2TiO_4. The lower endothermic peak of the doped sample represents the positive effects of Zn_2TiO_4 and benefits the dehydrogenation behaviour of MgH_2. It is important to note that the onset dehydrogenation temperatures obtained from DSC are higher than the curves determined by the PCT. The disparities could be attributed to the differences in heating rates and measuring atmospheres between PCT and DSC. The DSC was conducted at a heating rate of 25 °C/min with 50 mL/min Argon flow while the TPD experiment was conducted at a heating rate of 5 °C/min under vacuum. Similar outcomes were reported in previous studies [51–53].

Furthermore, to measure the enhancement of the dehydrogenation behaviour of MgH_2, the dehydrogenation activation energy (E_A) was evaluated by using Kissinger analysis as in Eq. (2) [54,55]:

$$\ln\left[\beta/T_p^2\right] = -E_A/RT_p + A \quad (2)$$

whereas,

β = heating rate used in the DSC measurements
T_p = temperature of the endothermic curve
R = gas constant
A = linear constant

As shown in Figs. 5(a) and 5(b), DSC experiments were performed at different heating rates to calculate E_A. Thereafter, the activation energy was calculated using the Kissinger plot of ln $[\beta/T_p^2]$ vs $1000/T_p$ as depicted in Fig. 5(c). As in Fig. 5(c), a satisfactory linear relationship between ln $[\beta/T_p^2]$ and $1000/T_p$ was established for the MgH_2 + 10 wt.% Zn_2TiO_4 sample and as-milled MgH_2. The calculated activation energy for the dehydrogenation process for the as-milled MgH_2 was 135 kJ/mol. The activation energy was lessened to 105.5 kJ/mol corresponding to a decrease of 22% to as-milled MgH_2 when Zn_2TiO_4 was added. This greatly reduces activation energy may be due to the particle sizes that have been reduced, which then minimises the distance for hydrogen diffusion and also broaden the specific surface area, favouring hydrogen transport and surface reaction [56]. These factors contribute to a significant decrease in operating temperatures.

In terms of thermodynamic properties, the DSC curves were analysed using the STARe software to calculate the enthalpy (ΔH_{dec}) of the decomposition of MgH_2. The enthalpy of the MgH_2 decomposition was determined from the integrated peak area. The hydrogen desorption enthalpy for the as-milled MgH_2 was found to be 75.7 kJ/mol H_2 which is matching the theoretical value (76 kJ/mol H_2) reported in a previous study [57]. The enthalpy of the MgH_2–Zn_2TiO_4 was similar to that of milled MgH_2. These outcomes agree with previous studies that reported that despite of enhancement in kinetic performance of MgH_2 by the addition of the catalyst, there was no impact on the thermodynamic of MgH_2 [58,59].

Fig. 6 presents the SEM images of the commercial MgH_2, as-milled MgH_2 and MgH_2 + 10 wt.% Zn_2TiO_4 sample. As can be seen in Fig. 6(a), the commercial MgH_2 consists of a large particle with a smooth surface whereas, after the 1 h of the ball milling (Fig. 6(b)), the as-milled MgH_2 presents a defect structure with a reduction of the particle size. Moreover, some agglomerations with non-uniform particle sizes were observed in as-milled MgH_2. These findings are in line with the previously reported in the literature [60], but the particle size was significantly reduced and become more homogenous after 10 wt.% Zn_2TiO_4 was added (Fig. 6(c)). Smaller and more homogenous particle size is vital in lowering the dehydrogenation temperature and improving the re/dehydrogenation kinetic characteristics of the MgH_2-catalysed system [49].

Fig. 7 depicts the particle size distribution of commercial MgH_2, as-milled MgH_2, and MgH_2 + 10 wt.% Zn_2TiO_4 samples quantified using Image J software. The average particle size of the commercial MgH_2 was calculated to be ~65 μm. Upon milling for 1 h, the average particle size of the

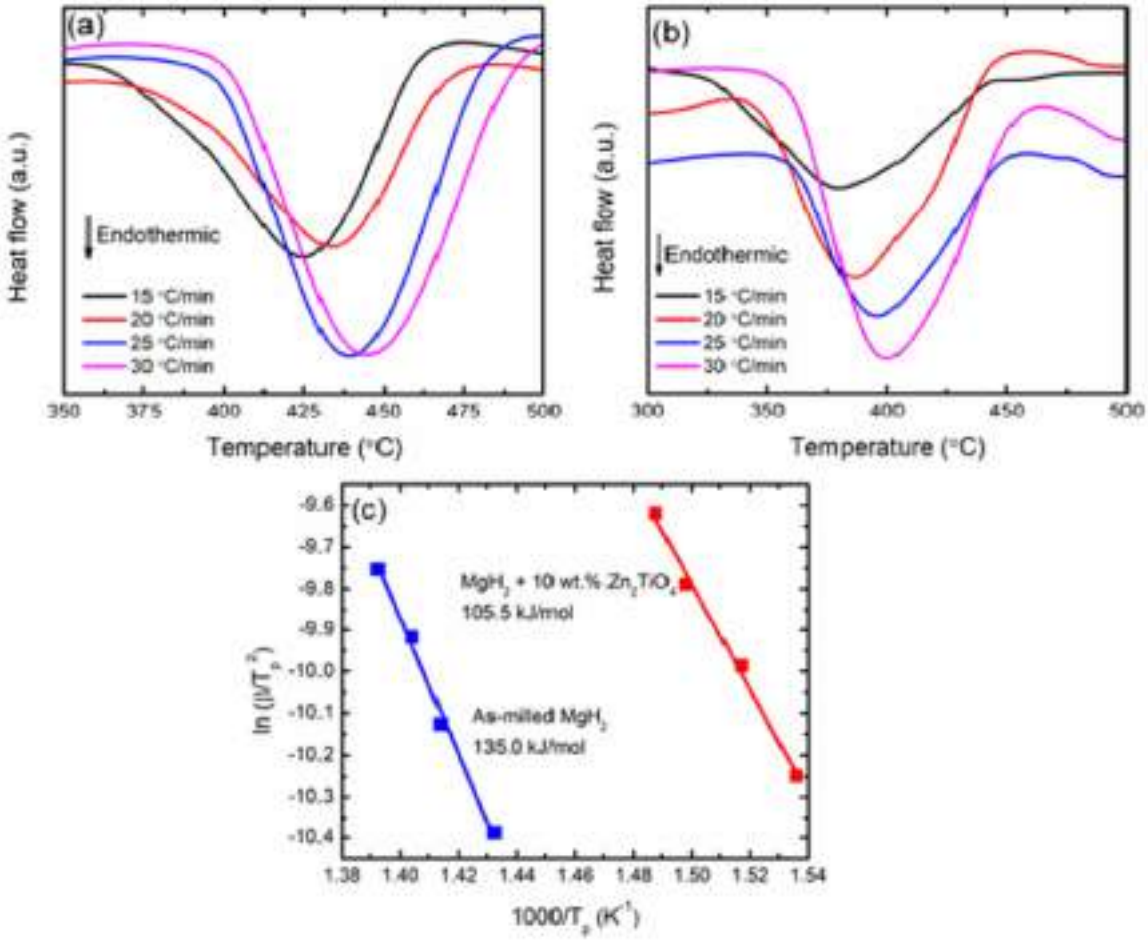

Fig. 5. DSC curve of (a) as-milled MgH_2, (b) MgH_2 + 10 wt.% Zn_2TiO_4 and (c) Kissinger plot of as-milled MgH_2 and MgH_2 + 10 wt.% Zn_2TiO_4.

as-milled MgH_2 was ~0.5 μm, which was significantly reduced compared to commercial MgH_2. The average particle size was significantly reduced to ~0.3 μm with the presence of Zn_2TiO_4. This demonstrates that the ball milling techniques and the inclusion of the Zn_2TiO_4 are beneficial in reducing the particle size of the MgH_2 + 10 wt.% Zn_2TiO_4 sample. The diffusion of H atoms to MgH_2 boundaries would be slower with larger particle sizes and fewer grain boundaries [61,62]. Hence, smaller particle sizes could reduce the length of hydrogen diffusion, thus accelerating the hydrogen storage behaviour of MgH_2.

The phase composition of the sample was then characterised using the XRD method, as shown in Fig. 8. The characterisation was performed in different states: a) after ball milling for 1 h, b) dehydrogenated state and c) rehydrogenated state. Referring to Fig. 8(a), MgH_2 peaks dominated the XRD patterns with several peaks of Zn_2TiO_4. There was no new peak recorded, demonstrating that there was no chemical reaction throughout the ball milling process. For the dehydrogenated state (Fig. 8(b)), all MgH_2 peaks vanished and Mg peaks formed presenting the complete dehydrogenation of MgH_2. Additional peaks of MgO, $MgTiO_3$ and $MgZn_2$ appear showing that a chemical reaction occurred during the heating process. For the rehydrogenated state, similar peaks are obtained with the exception of the Mg peaks that are supplanted by the MgH_2 peaks (Fig. 8(c)).

The XRD measurement for the 20 wt.% Zn_2TiO_4-doped MgH_2 sample was performed as shown in Fig. 9 to confirm the reaction that happens during the milling process and after re/dehydrogenation process. After milling for 1 h (Fig. 9(a)), the only peaks available are the peaks of MgH_2 and Zn_2TiO_4. For the dehydrogenated state (Fig. 9(b)), the peaks available are the peaks of Mg indicating the complete dehydrogenation of MgH_2 with the additional peaks of MgO, $MgTiO_3$ and $MgZn_2$. The peaks of MgO, $MgTiO_3$ and $MgZn_2$ remain unaltered for the rehydrogenated state (Fig. 9(c)), and the Mg peaks are supplanted by the MgH_2 peaks. The presence of MgH_2 peaks indicates the reversibility of Mg, which is one of the most significant indicators for hydrogen storage. Based on this XRD analysis, a probable reaction that took place during the heating process is best summarised as follows:

$$9MgH_2 + 3Zn_2TiO_4 \rightarrow 3MgO + 3MgZn_2 + 3MgTiO_3 + 9H_2 \quad (3)$$

Referring to the XRD analysis, the enhanced kinetics of MgH_2 doped with Zn_2TiO_4 are benefited by the formation of new active species of MgO, $MgTiO_3$ and $MgZn_2$. These active species function as an active channel at the MgH_2 matrix's surface, providing a rapid pathway for the H atom to diffuse throughout the re/dehydrogenation processes [16,63]. For instance, Ares-Fernandez and Aguey-Zinsou [64] found

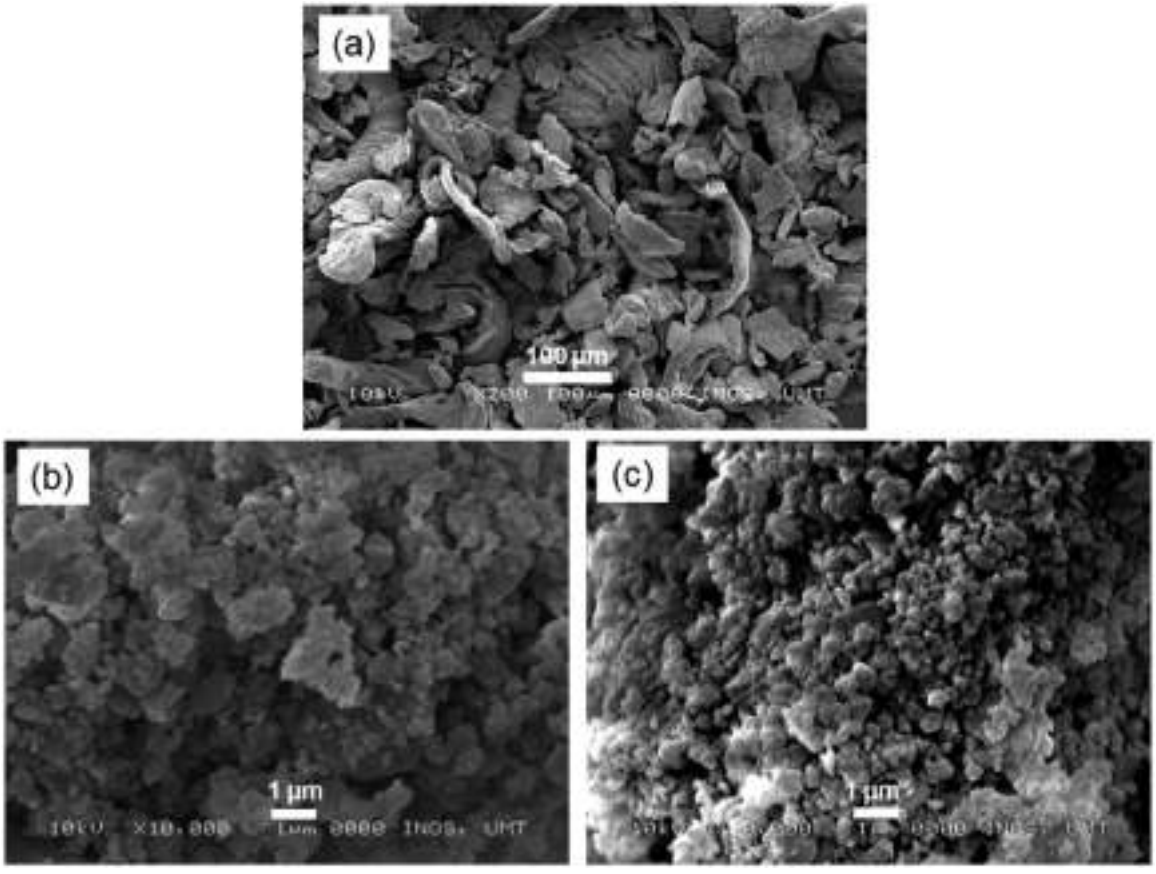

Fig. 6. The SEM profiles of (a) commercial MgH_2, (b) as-milled MgH_2 and (c) MgH_2 + 10 wt.% Zn_2TiO_4.

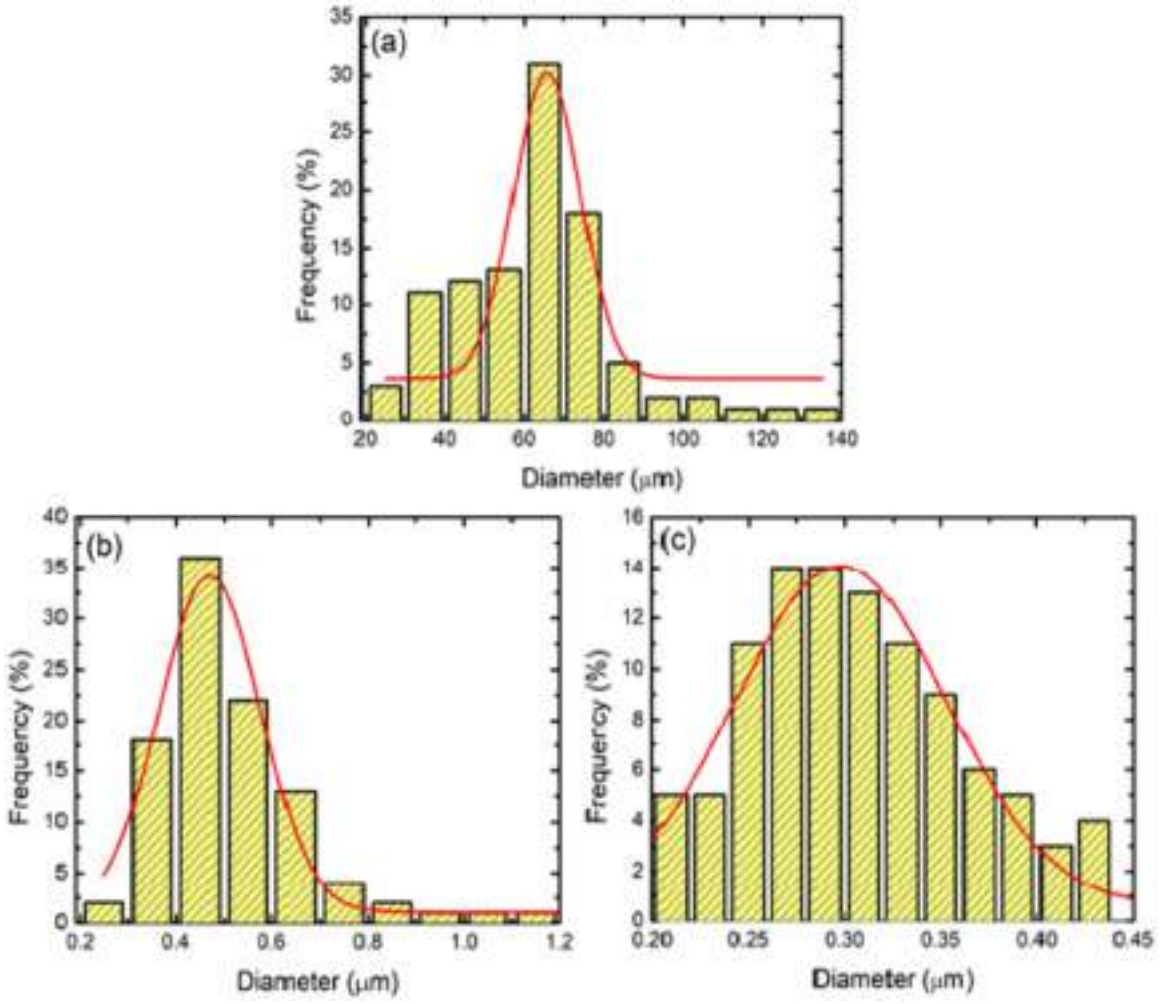

Fig. 7. Histogram of the particle size distribution of (a) commercial MgH_2, (b) as-milled MgH_2 and (c) MgH_2 + 10 wt.% Zn_2TiO_4.

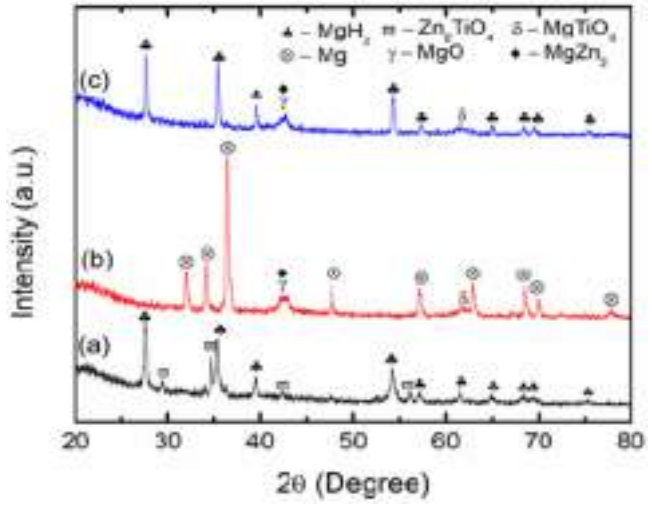

Fig. 8. The XRD pattern of the (a) as-milled, (b) dehydrogenated state and (c) rehydrogenated state of MgH_2 + 10 wt.% Zn_2TiO_4.

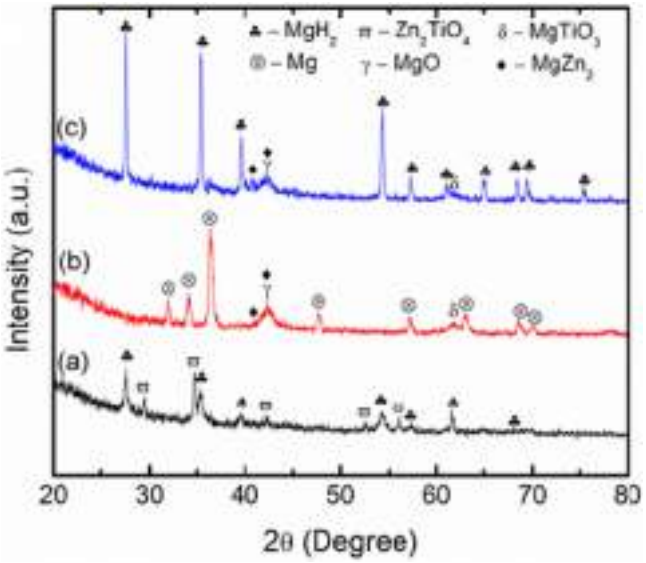

Fig. 9. The XRD pattern of the (a) as-milled, (b) dehydrogenated state and (c) rehydrogenated state of MgH_2 + 20 wt.% Zn_2TiO_4.

that MgO can act as a control process agent, reducing and preventing MgH_2 agglomeration by attaining an ideal breakage rate. In addition, the presence of $MgTiO_3$ performs superior kinetics performance of MgH_2 with the ability to absorb 5.0 wt.% H_2 in 500 s [65]. Other research also indicates that the presence of $MgZn_2$ can assist hydrogen diffusion and promotes structural defects (such as lattice dislocations and grain boundaries) [66,67]. Moreover, the in situ formation of $MgZn_2$ benefited the hydrogen storage performance of the $Mg_{95}Sn_3Zn_2$ alloy [68]. According to another study, $Mg_{0.97}Zn_{0.03}$ is converted into MgH_2 and intermetallic $MgZn_2$ compounds during the early phases of the hydrogenation process [69]. During dehydrogenation, the generated $MgZn_2$ nanoparticles were converted to an Mg(Zn) solid solution, which was distributed homogenously in the MgH_2 matrix. This intriguing reversible phase change of Mg(Zn) benefits substantially from the decrease in the thermodynamic stability of MgH_2 [70]. As a consequence, the catalytic effects of $MgZn_2$, $MgTiO_3$ and MgO could collaborate to further boost the re/dehydrogenation kinetics of MgH_2 as well as lower the dehydrogenation temperature. However, to assess the overall impact and mechanism of the MgH_2–Zn_2TiO_4 system, more characterization employing transmission electron microscopy and X-ray photoelectron spectroscopy is required.

4. Conclusions

The inclusion of solid-state synthesized Zn_2TiO_4 benefited the hydrogen storage behaviour of MgH_2. By adding different wt.% of Zn_2TiO_4, the initial dehydrogenation temperature of MgH_2 was downshifted to around 290 °C–305 °C. The kinetics behaviour of the MgH_2 was also boosted with the capability to absorb 5.0 wt.% H_2 by the MgH_2–Zn_2TiO_4 sample at 250 °C within 300 s and liberates 2.2–3.6 wt.% H_2 from the composite sample at 300 °C within 30 min. The dehydrogenation activation energy of the MgH_2–Zn_2TiO_4 system was also reduced by 22% than undoped MgH_2. The excellent hydrogen storage behaviour of the MgH_2–Zn_2TiO_4 system is corresponding to the synergistic effect of MgO, $MgTiO_3$ and $MgZn_2$ that formed in situ during the heating process that is beneficial in ameliorating the re/dehydrogenation behaviour of MgH_2. From the result, it can be deduced that the solid-state synthesized Zn_2TiO_4 is a promising additive to boost the hydrogen storage behaviour of MgH_2. These findings may be advantageous modifications to the MgH_2 system.

Acknowledgment

The authors acknowledged Universiti Malaysia Terengganu (UMT) for the funding provided by Golden Goose Research Grant (GGRG) VOT 55190. N. A. Ali and N. A. Sazelee are thankful UMT for the SIPP and BUMT scholarship. M. Ismail, M. M. Nasef and A. A. Jalil also thank the Prominent Visiting Researcher Scheme awarded by The Department of Deputy Vice Chancellor (Research & Innovation), Universiti Teknologi Malaysia.

References

[1] Q. Hou, X. Yang, J. Zhang, Chemistry Select 6 (2021) 1589–1606.
[2] Y. Shang, C. Pistidda, G. Gizer, T. Klassen, M. Dornheim, J Magnes Alloy 9 (2021) 1837–1860.
[3] N.A. Ali, M. Ismail, J Magnes Alloy 9 (2021) 1111–1122.
[4] L. Ouyang, F. Liu, H. Wang, J. Liu, X.-S. Yang, et al., J Alloy Compd 832 (2020) 154865.
[5] P. Thongtan, S. Thiangviriya, O. Utke, R. Utke, J Phys Chem Solids 163 (2022) 110578.
[6] X. Zhang, Y. Liu, Z. Ren, X. Zhang, J. Hu, et al., Energy Environ Sci 14 (2021) 2302–2313.
[7] N.A. Ali, N.A. Sazelee, M. Ismail, Int J Hydrog Energy 46 (2021) 31674–31698.
[8] Q. Hou, J. Zhang, X. Guo, X. Yang, J Taiwan Inst Chem Eng J 134 (2022) 104311.
[9] H. Gao, R. Shi, Y. Shao, Y. Liu, Y. Zhu, et al., Int J Hydrog Energy 47 (2022) 9346–9356.
[10] F.A. Halim Yap, N.S. Mustafa, M. Ismail, RSC Adv 5 (2015) 9255–9260.
[11] W. Liao, W. Jiang, X.-S. Yang, H. Wang, L. Ouyang, et al., J Rare Earths 39 (2021) 1010–1016.
[12] X.L. Zhang, Y.F. Liu, X. Zhang, J.J. Hu, M.X. Gao, et al., Mater Today Nano 9 (2020) 100064.
[13] M. Ismail, Int J Hydrog Energy 46 (2021) 8621–8628.
[14] S.D. House, J.J. Vajo, C. Ren, A.A. Rockett, I.M. Robertson, Acta Mater 86 (2015) 55–68.
[15] N. Sazelee, M.F. Md Din, M. Ismail, Materials 16 (2023) 2176.
[16] P. Wang, Z. Tian, Z. Wang, C. Xia, T. Yang, et al., Int J Hydrog Energy 46 (2021) 27107–27118.
[17] N.A. Sazelee, N.H. Idris, M.F. Md Din, M.S. Yahya, N.A. Ali, et al., Results Phys 16 (2020) 102844.
[18] L. Ren, W. Zhu, Q. Zhang, C. Lu, F. Sun, et al., Chem Eng 434 (2022) 134701.
[19] N.S. Mustafa, M. Ismail, Int J Hydrog Energy 39 (2014) 15563–15569.
[20] H. Gao, R. Shi, Y. Shao, Y. Liu, Y. Zhu, et al., J Alloy Compd 895 (2022) 162635.
[21] N. Hanada, T. Ichikawa, H. Fujii, J Phys Chem B 109 (2005) 7188–7194.
[22] A. Roy, A. Janotti, C.G. Van de Walle, Appl Phys Lett 102 (2013) 033902.
[23] A. Rahwanto, I. Ismail, N. Nurmalita, Mustanir, Z. Jalil, J Phys Conf Ser 1882 (2021) 012010.
[24] M. Malahayati, N. Nurmalita, I. Ismail, M.N. Machmud, Z. Jalil, J Phys Conf Ser 1882 (2021) 012005.
[25] A. Rahwanto, Z. Jalil, Akhyar, E. Handoko, IOP Conf Ser Mater Sci Eng 931 (2020) 012012.
[26] S. Gao, X. Wang, H. Liu, T. He, Y. Wang, et al., Int J Hydrog Energy 45 (2020) 28964–28973.
[27] M. Chen, X. Xiao, X. Wang, Y. Lu, M. Zhang, et al., Carbon 166 (2020) 46–55.
[28] C. Milanese, A. Girella, S. Garroni, G. Bruni, V. Berbenni, et al., Int J Hydrog Energy 35 (2010) 9027–9037.
[29] C. Milanese, A. Girella, S. Garroni, G. Bruni, V. Berbenni, et al., Nanosci Nanotechnol Lett 4 (2012) 195–204.
[30] X. Huang, X. Xiao, X. Wang, C. Wang, X. Fan, et al., J Phys Chem C 122 (2018) 27973–27982.
[31] M.S. Yahya, M. Ismail, J Energy Chem 28 (2019) 46–53.
[32] N. Yan, X. Lu, Z. Lu, H. Yu, F. Wu, et al., J Magnes Alloy (2021) 3542–3552.
[33] S. Hu, H. Zhang, Z. Yuan, Y. Wang, G. Fan, et al., J Alloy Compd 881 (2021) 160571.
[34] Q. Kong, H. Zhang, Z. Yuan, J. Liu, L. Li, et al., ACS Sustain Chem Eng 8 (2020) 4755–4763.
[35] Y. Shao, H. Gao, Q. Tang, Y. Liu, J. Liu, et al., Appl Surf Sci 585 (2022) 152561.
[36] M. Zhang, X. Xiao, X. Wang, M. Chen, Y. Lu, et al., Nanoscale 11 (2019) 7465–7473.

[37] M. Zhang, X. Xiao, J. Mao, Z. Lan, X. Huang, et al., Mater Today Energy 12 (2019) 146–154.
[38] M. Chen, X. Xiao, M. Zhang, J. Mao, J. Zheng, et al., Mater Today Energy 16 (2020) 100411.
[39] M.C. Han, L.L. Zhu, S.Y. Jiao, T.F. Yi, P. Cui, et al., Adv Sustain Syst 5 (2021) 2100149.
[40] K.M. Girish, S.C. Prashantha, H. Nagabhushana, C.R. Ravikumar, H.P. Nagaswarupa, et al., J Sci 3 (2018) 151–160.
[41] P. Danwanichakul, T. Suwatthanarak, C. Suwanvisith, D. Danwanichakul, J Nanosci 2016 (2016) 7258313.
[42] J. Wang, A. Sugawara-Narutaki, M. Fukao, T. Yokoi, A. Shimojima, et al., ACS Appl Mater Interfaces 3 (2011) 1538–1544.
[43] T. Riaz, N. Assey, M. Javed, T. Shahzadi, M. Zaib, et al., Inorg Chem Commun 140 (2022) 109449.
[44] R.B. Pinto, P. Peralta-Zamora, F. Wypych, J Photochem Photobiol A 353 (2018) 46–52.
[45] A. Mebrek, S. Alleg, S. Benayache, M. Benabdeslem, Ceram Int 44 (2018) 10921–10928.
[46] L. Perfler, V. Kahlenberg, G. Jakopic, A. Schaur, M. Tribus, et al., Mater Res Bull 95 (2017) 367–379.
[47] Z. Wang, S.K. Saxena, C.S. Zha, Phys Rev B 66 (2002) 024103.
[48] N. Sazelee, N. Idris, M.M. Din, N. Mustafa, N. Ali, et al., Int J Hydrog Energy 43 (2018) 20853–20860.
[49] N.A. Ali, M.S. Yahya, N. Sazelee, M.F.M. Din, M. Ismail, Nanomaterials 12 (2022) 3043.
[50] G. Tian, F. Wu, H. Zhang, J. Wei, H. Zhao, et al., J Phys Chem Solids 174 (2023) 111187.
[51] Q. Wan, P. Li, J. Shan, F. Zhai, Z. Li, et al., J Phys Chem C 119 (2015) 2925–2934.
[52] M.-Q. Fan, S.-s. Liu, Y. Zhang, J. Zhang, L.-X. Sun, et al., Energy 35 (2010) 3417–3421.
[53] M. Yahya, N. Sulaiman, N. Mustafa, F.H. Yap, M. Ismail, Int J Hydrog Energy 43 (2018) 14532–14540.
[54] X. Shen, X. Zhang, Q. Xiao, H. Liu, Int J Hydrog Energy 47 (2022) 16964–16977.
[55] J. Cermak, L. Kral, P. Roupcova, Renew Energy 188 (2022) 411–424.
[56] X. Zhang, W. Zhang, L. Zhang, Z. Huang, J. Hu, et al., Chem Eng 428 (2022) 132566.
[57] Z. Yuan, S. Li, K. Wang, N. Xu, W. Sun, et al., Chem Eng 435 (2022) 135050.
[58] S.A. Shevlin, Z.X. Guo, J Phys Chem C 117 (2013) 10883–10891.
[59] S.K. Pandey, A. Bhatnagar, V. Shukla, R. Kesarwani, U. Deshpandey, et al., Int J Hydrog Energy 46 (2021) 37340–37350.
[60] K.C. Tome, S. Xi, Y. Fu, C. Lu, N. Lu, et al., Int J Hydrog Energy 47 (2021) 4716–4724.
[61] X. Ding, R. Chen, J. Zhang, W. Cao, Y. Su, et al., J Alloy Compd 897 (2022) 163137.
[62] J. Yao, Y. Zhao, H. Yong, S. Wang, T. Han, et al., J Phys Chem Solids 174 (2023) 111153.
[63] I. Malka, M. Pisarek, T. Czujko, J. Bystrzycki, Int J Hydrog Energy 36 (2011) 12909–12917.
[64] K.F. Aguey-Zinsou, J.R. Ares Fernandez, T. Klassen, R. Bormann, Mater Res Bull 41 (2006) 1118–1126.
[65] D. Pukazhselvan, N. Nasani, T. Yang, D. Ramasamy, A. Shaula, et al., Appl Surf Sci 472 (2019) 99–104.
[66] Z. Yuan, Y. Sui, T. Zhai, Y. Yin, L. Luo, et al., Mater Charact 178 (2021) 111248.
[67] Y. Yin, B. Li, Z. Yuan, Y. Qi, Y. Zhang, J Phys Chem Solids 134 (2019) 295–306.
[68] H.C. Zhong, J.B. Xu, Int J Hydrog Energy 44 (2019) 2926–2933.
[69] H. Zhong, Y. Huang, Z. Du, H. Lin, X. Lu, et al., Int J Hydrog Energy 45 (2020) 27404–27412.
[70] C.N.C. Hitam, M.A.A. Aziz, A.H. Ruhaimi, M.R. Taib, Int J Hydrog Energy 46 (2021) 31067–31083.